MAGNETOHYDRODYNAMIC IONIZING SHOCK WAVES IN A CONDUCTING MEDIUM

By B. GREEN* and R. M. MAY*

[*Manuscript received March* 9, 1965]

Summary

We present numerical calculations for the flow parameters (velocity, density, pressure, etc.) in a magnetohydrodynamic shock wave propagating in a conducting medium. The effect of ionization in the shock front is included. The results are presented graphically for a complete range of the initial magnetic field strength and direction, and for several arbitrary values of the ionization energy of the downstream fluid.

I. INTRODUCTION

Kemp and Petschek (1959) (hereafter called K.P.) have made a detailed investigation of the propagation of a magnetohydrodynamic shock wave in a conducting medium. Following methods made familiar by the study of ordinary gas dynamic shocks, K.P. divide the flow into four regions: the undisturbed gas ahead of the shock front; the steady flow region behind the shock front (containing the high temperature gas sample suitable for plasma studies); the expansion wave; and the steady flow region behind the expansion wave, which joins to the boundary conditions at the end of the shock tube. K.P. derive quantitative results for the variation of all flow parameters (velocity, density, temperature, etc.) throughout all these regions. They consider arbitrary orientation of the magnetic field ahead of the shock front: in this regard their work is an extension of that of Bazer (1958), who considers a purely axial field ahead of the front.

In the present paper, we extend the work of K.P. by including the possibility of a change in internal energy of the gas through the shock front. Such an internal energy change would occur, for example, if the conducting gas were further ionized by the passage of the shock wave.

It is to be emphasized that both K.P. and the present work assume that the gas ahead of the shock front is "conducting". The case of an ionizing magnetohydrodynamic shock wave propagating into a "non-conducting" medium, is much more complex (Kulikovski and Lyubimov 1960; Gross and Kunkel 1962; Chu 1964; May and Tendys 1965). We need only note that the criterion (May and Tendys 1965) for the undisturbed gas ahead of the front to be deemed "conducting" is that its magnetic diffusivity $1/\sigma\mu$ be very much less than its viscosity ν and thermal conductivity κ (see Lehnert 1958 for a table giving ν, κ, and $1/\mu\sigma$ for several gases at various densities and temperatures), that is,

$$1/\mu\sigma \ll \nu, \kappa. \tag{1}$$

This criterion can well be fulfilled even if the gas ahead of the shock front is only

* Theoretical Department, School of Physics, University of Sydney.

partly ionized (e.g. in a gas of hydrogen at density 10^{16} molecules/cm^3, the criterion is fulfilled at 2% ionization). Thus there is some practical point in extending the analysis of K.P. to include the possibility of further ionization of an already "conducting" gas by the passage of a magnetohydrodynamic shock wave.*

In Section II we describe the equations and method of treatment used to derive our results for the various flow parameters. Since the analysis is very similar to that of K.P., we confine ourselves to an outline. In Section III, the results are presented and discussed. These results are mainly in the form of a series of graphs for the various flow quantities.

Before proceeding to the results, we mention the recent work of Taussig (1964), who has also introduced the internal energy change term into a study of magnetohydrodynamic ionizing shock waves. However, Taussig considers only "normal" shocks in which the magnetic field in the undisturbed region ahead of the shock

TABLE 1

COMPARISON OF PRESENT WORK WITH THAT OF EARLIER AUTHORS

Authors	Angle of Initial Magnetic Field θ (from eqn. (2))	Conductivity ahead of Shock Front	Internal Energy Change through Shock Front
Bazer (1958)	0	∞	0
Kemp and Petschek (1959)	$0<\theta<\frac{1}{2}\pi$	∞	0
Taussig (1964)	0	finite	finite
Present work	$0<\theta<\frac{1}{2}\pi$	∞	finite

front is perpendicular to the front; while we (as did K.P.) consider arbitrary orientations of this field, that is, we have $\frac{1}{2}\pi \geqslant \theta \geqslant 0$ (Taussig has $\theta = 0$), where θ is defined by equation (2) in Section II. On the other hand, we restrict ourselves to conducting media, so that ahead of the shock front we must have the electric field zero; whereas Taussig considers the general case where the medium ahead of the shock front need not be conducting, and hence the electric field need not be zero. The relation between the present work and that of Taussig and earlier authors is summarized schematically in Table 1.

II. ANALYSIS

Since our program differs from that of K.P. only by the inclusion of a change in internal energy through the shock front, we present only an outline of the method of analysis and refer to K.P. for details.

We consider plane flow in the X–Y plane, with all the flow quantities being functions only of the variable X. This idealization gives a reasonable approximation to the usual experimental conditions of flow in the annulus between two concentric

* In the AVCO experiments considered by K.P., and all other similar experiments so far performed, the analysis that ignores internal energy changes is adequate, either because the gas ahead of the front is already fully ionized, or because the temperatures behind the front are sufficiently large to dwarf the internal energy change.

cylinders. X corresponds to the axial, Y to the azimuthal, and Z to the radial direction. It is also assumed that the gas pressure is isotropic, and that the criterion (1) is satisfied so that the medium is conducting ahead of the shock front. All calculations are made in a reference frame attached to the shock front.

The analytical solution of the problem has five parameters which may be chosen as:

(*a*) The angle of orientation θ of the initial magnetic field,

$$\theta = \tan^{-1}(B_{Y1}/B_X), \tag{2}$$

where B_{Y1} is the azimuthal magnetic field ahead of the shock (region 1), and B_X is the axial field, which is constant ($\nabla.\mathbf{B} = 0$).

(*b*) The ratio of the shock speed U_S to the fast sound speed c_f in the undisturbed gas ahead of the shock front, i.e. the ratio U_S/c_f.

(*c*) The ratio of gas pressure to magnetic pressure in the undisturbed gas, i.e. the ratio $p_1/(B_1^2/2\mu)$. B_1 is the modulus of the magnetic field in region 1, or $B_1^2 = B_{Y1}^2+B_X^2$.

(*d*) The ratio of specific heats γ in the ionized gas behind the shock.

(*e*) The ratio P of the change in internal energy through the shock front to the magnetic energy ahead of the front,

$$P = \rho_1 \mu(\Delta e)/B_1^2. \tag{3}$$

In the limit $P = 0$, our calculations reduce to those of K.P.

Although the general theory is valid for arbitrary values of these parameters, in order to perform the numerical computations, we have specified the parameters (*c*) and (*d*) by choosing

$$p_1/(B_1^2/2\mu) = 0 \tag{4}$$

and

$$\gamma = 5/3. \tag{5}$$

Both these choices will be good approximations to most experimental conditions. Notice that the choice (4) implies that the fast sound speed c_f is now the Alfven speed, that is, $c_f = (B_1^2/\rho_1 \mu)^{\frac{1}{2}}$.

With the simplifications described above, the flow becomes one of a perfect gas with infinite conductivity. In the reference frame we have chosen, physical quantities vary only with X; the velocity and magnetic field vectors have only X components (u, B_X) and Y components (v, B_Y); the fluid pressure and density are p and ρ respectively. (We use rationalized MKS units, with μ denoting the permeability of free space.) The appropriate differential equations for the flow and the magnetic field are now Maxwell's equations and the compressible, perfect gas, fluid-flow equations with the magnetic force and energy terms added.

Figure 1 is a displacement–time diagram showing the various flow regions of the shock wave. For the equations relating quantities ahead of the shock front (region 1) to those behind the front (region 2), we have the usual jump relations, which express conservation of mass, longitudinal and transverse momentum, and energy. Our inclusion of a change in internal energy through the front alters only the energy equation; all the other equations remain as in K.P. Allowing for a change in internal energy, Δe, the energy conservation equation (K.P. equation (24)) now reads

$$\rho_1 u_1\left\{\frac{\gamma}{\gamma-1}\frac{p_1}{\rho_1}+\tfrac{1}{2}(u_1^2+v_1^2)\right\}+\frac{B_{Y1}}{\mu}(B_{Y1}u_1-B_X v_1)$$

$$=\rho_2 u_2\left\{\frac{\gamma}{\gamma-1}\frac{p_2}{\rho_2}+\tfrac{1}{2}(u_2^2+v_2^2)+\Delta e\right\}+\frac{B_{Y2}}{\mu}(B_{Y2}u_2-B_X v_2). \qquad (6)$$

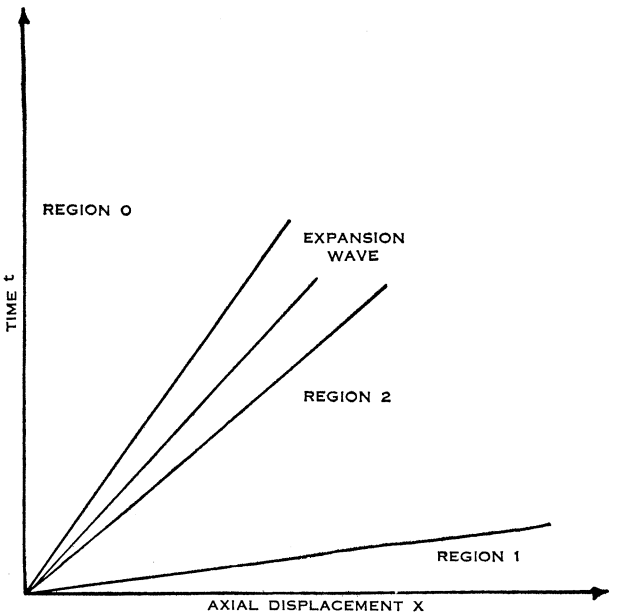

Fig. 1.—X–t diagram showing flow regions.

The suffix 1 denotes region 1 ahead of the front, and the suffix 2 denotes region 2. The other jump relations connecting the flow parameters in region 1 to those in region 2 are identical with K.P. equations (19)–(23).

The steady flow region 2 behind the shock front is joined to the back of the shock tube (region 0) by a simple expansion wave. We assume that no further change in internal energy takes place behind the shock front.* Thus the expansion wave is described by the K.P. set of three simultaneous first-order differential equations, together with one algebraic equation (K.P. equations (9)–(12)). This set of equations

* This point is discussed further by Taussig (1965).

is solved by numerical integration, beginning from region 2 and terminating with a boundary condition enforced by the back wall of the shock tube, namely, that in the laboratory frame there should be no axial motion in region 0. This boundary condition can be achieved either

(i) by a vacuum in region 0 ($p_0 = 0$, $\rho_0 = 0$), or

(ii) by having no axial flow in region 0 ($u_0 = U_S$ in the shock-centred frame).

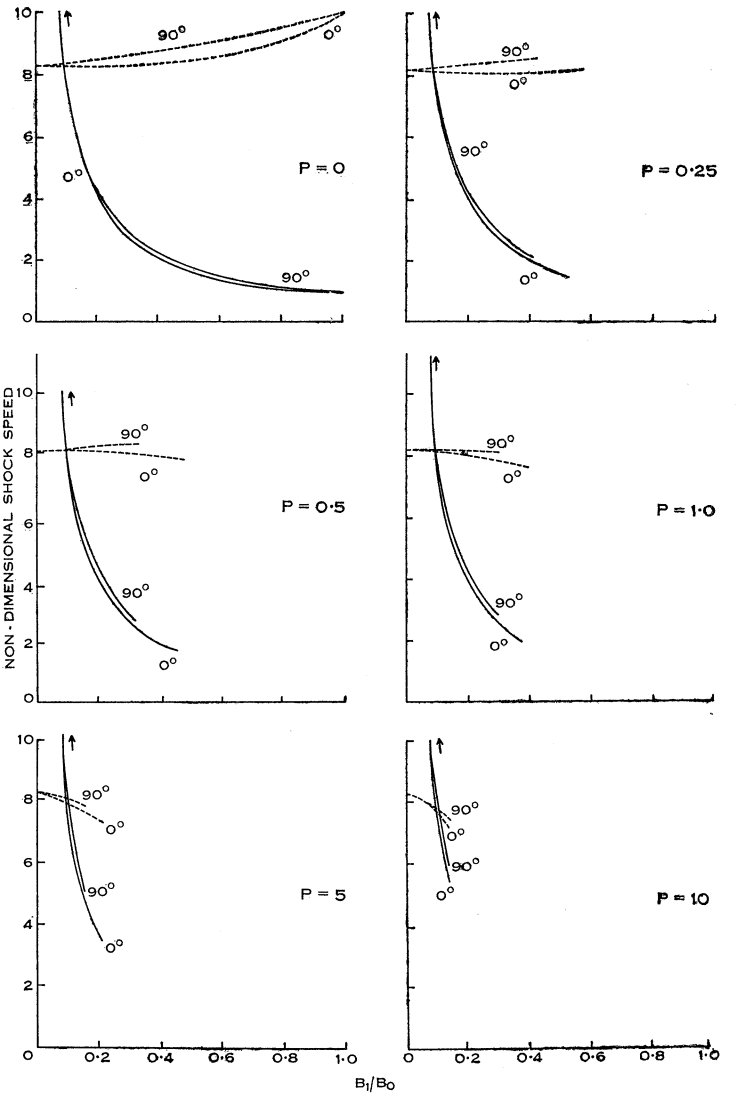

Fig. 2.—Non-dimensional shock speed U_S/b_1 (solid curves) and $10U_S/b_*$ (dashed curves) versus B_1/B_0 for $\theta = 0$ and 90°, and various values of P.

Thus a complete solution for the flow parameters in all regions is obtained by first specifying the five parameters (*a*)–(*e*) above, then obtaining the flow in region 2

behind the shock front by using the jump relations described above, and finally obtaining the flow in region 0 by integration through the expansion wave. We now proceed to the results obtained from this program.

III. Results

The results for the significant flow parameters in various regions are plotted against the ratio B_1/B_0, where B_1 is the magnitude of the field ahead of the shock front, and B_0 is the magnitude of the field at the back wall. We occasionally refer to the "drive field", by which we mean the difference B_0-B_1. Each parameter is plotted against B_1/B_0 for several values of the remaining parameters θ (equation (2)) and P (equation (3)).

The qualitative and quantitative behaviour of the flow with $\frac{1}{2}\pi > \theta > 0$ is bounded by the extreme cases of $\theta = 0$ and $\theta = \frac{1}{2}\pi$. The $\theta = \frac{1}{2}\pi$ case, corresponding to a magnetic field completely parallel to the shock front, presents a simple picture, namely, a piston-like shock wave moving down the tube causing axial motion of the gas ahead of it. The $\theta = 0$ case, corresponding to a magnetic field completely perpendicular to the wave front, is more complicated and there are now two possible flow regimes. If the azimuthal field B_{Y2} is finite behind the front, we get the "switch-on" shock with its associated fluid rotation behind the front; if $B_{Y2} = 0$, the flow is as in an ordinary gas dynamic shock.

Comparison of the results for finite internal energy changes, $P \neq 0$, with the special case $P = 0$ shows the existence of a restriction on the permissible values of B_1/B_0. (We recall that P represents a change in internal energy, due to an increase in ionization.) Values of B_1/B_0 that correspond to a non-physical negative temperature in region 2 have been discarded; they correspond to values of the drive field B_0-B_1 that are too small to impart enough energy to the shock wave to provide the required internal energy change.

Another difference between the cases $P \neq 0$ and $P = 0$ occurs in the boundary condition enforced at the back wall of the shock tube. For $P = 0$, K.P. find that this boundary condition is sometimes satisfied by having no axial gas motion in region 0, although more often it is only satisfied by having a vacuum in region 0; for $P \neq 0$ the latter condition always prevails.

We now make itemized comments on the graphs, Figures 2–10.

Figure 2 displays the (non-dimensional) shock speed. This shock speed is made non-dimensional in two different ways.

(i) U_S/b_1, where b_1 is the Alfven speed ahead of the front, that is, $b_1 = (B_1^2/\rho_1\mu)^{\frac{1}{2}}$. It is seen that greater drive fields (B_0-B_1) are required to produce greater ionization when the initial magnetic field B_1 and the shock speed are fixed.

(ii) U_S/b_*, where $b_* = (B_0^2/\rho_1\mu)^{\frac{1}{2}}$. These curves show small variation with B_1/B_0. However, for a fixed U_S and B_0, smaller initial fields B_1 (i.e. greater drive fields, as before) are required to produce greater ionization. As in K.P., the limiting value of this quantity for $B_1/B_0 = 0$ can be calculated. For $P = 0$ this limit is approximately 8·16, and for $P \neq 0$ and increasing, this limit decreases slowly.

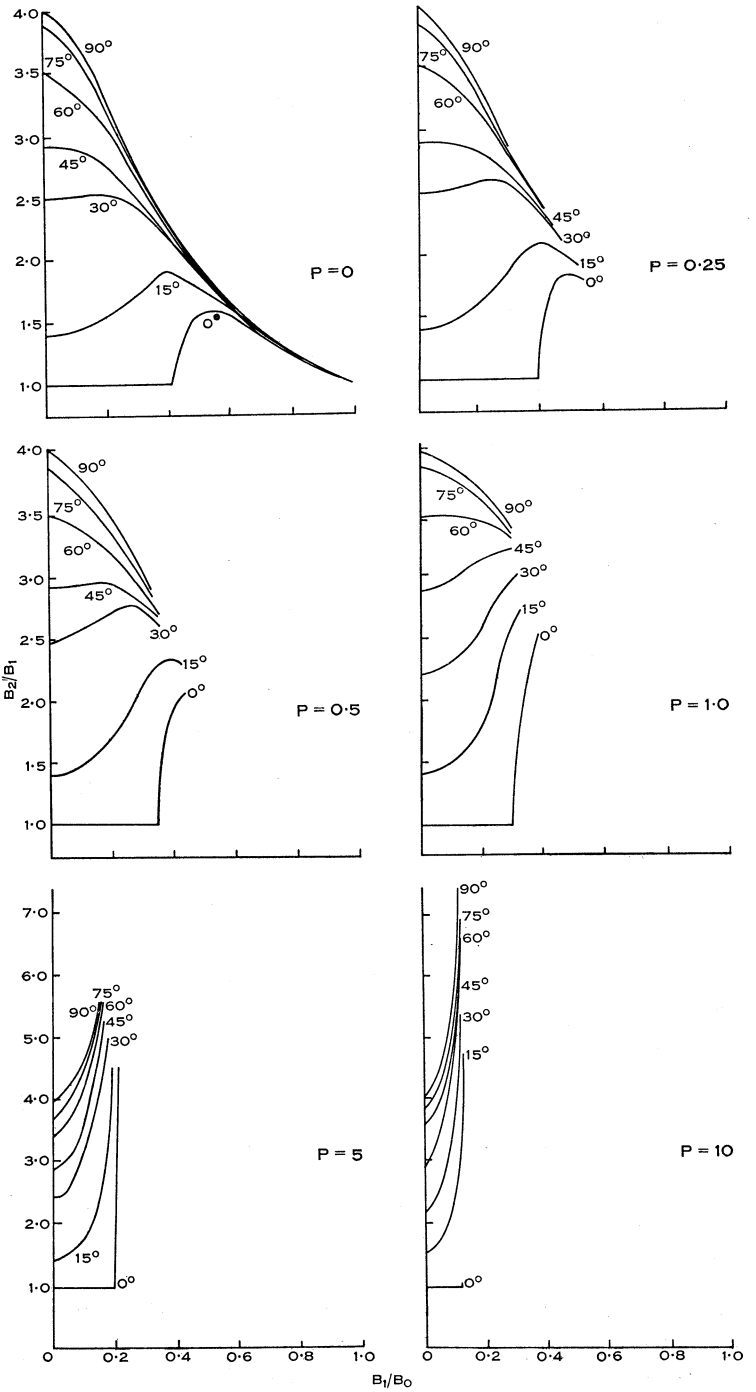

Fig. 3.—Magnetic field strength ratio across the shock, B_2/B_1, versus B_1/B_0 for various values of θ and P.

The "knee" in the B_2/B_1 curves (Fig. 3), clearly seen for most of the $\theta = 0$ cases, gives the transition between the switch-on and ordinary shock regions. These latter regions lie towards lower B_1/B_0 values. This transition cannot be seen for the $P = 10$ curve, because the physical switch-on region is now very small; the non-physical portion continually expands as the value of P is increased, until it almost

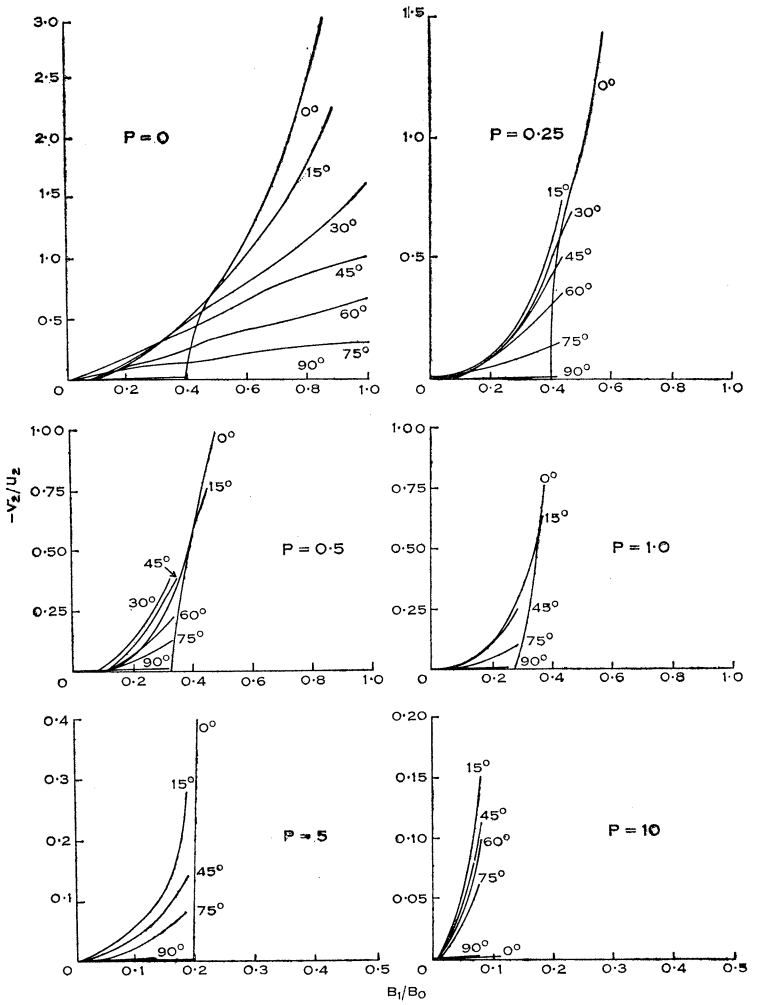

Fig. 4.—Negative tangent of the flow angle behind the shock wave, $-v_2/u_2$ (in laboratory coordinates), versus B_1/B_0 for various values of θ and P.

fills the total switch-on shock region. For the transverse shock ($\theta = 90°$), there is a stage reached where B_2/B_1 and ρ_2/ρ_1 no longer decrease for increasing B_1/B_0 but increase, i.e. the shock becomes highly compressive. Similarly for the other θ values, the maxima of the lower θ curves disappear as P increases until all θ curves are strictly increasing with increasing B_1/B_0. Conversely, very high ionization energy values

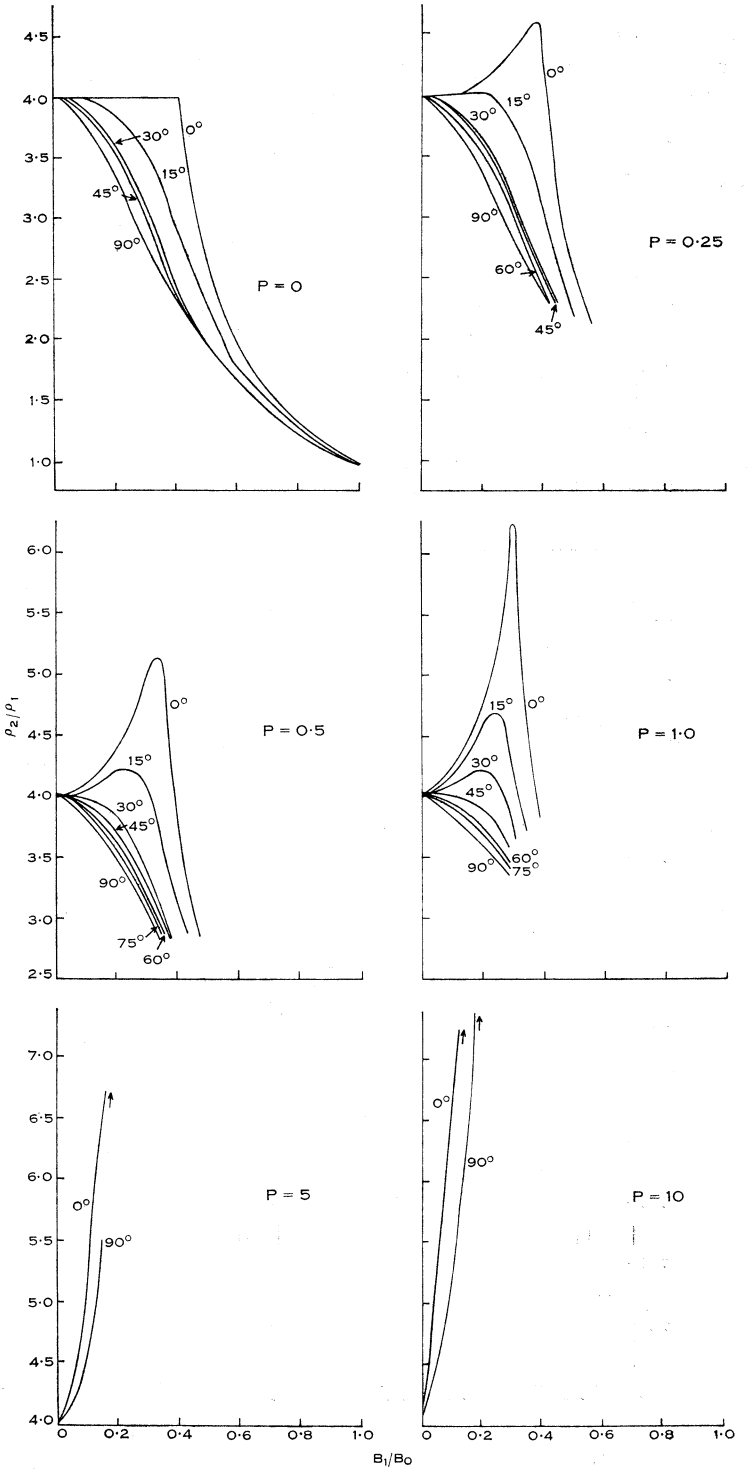

Fig. 5.—Density ratio across the shock wave, ρ_2/ρ_1, versus B_1/B_0 for various values of θ and P.

can be produced by highly compressive (i.e. very strong) shock waves. The limiting values for B_2/B_1 and ρ_2/ρ_1 when $B_1/B_0 = 0$ are slightly increased on increasing P (all $\theta \neq 0$).

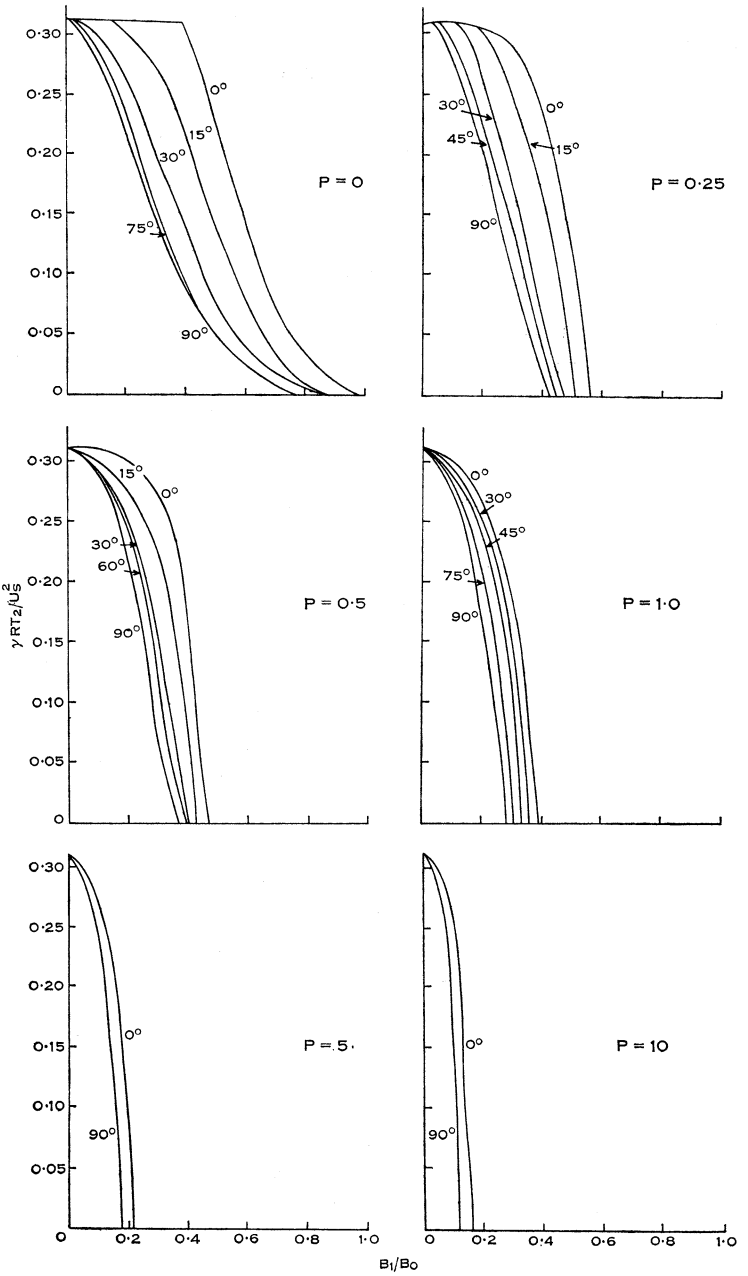

Fig. 6.—Non-dimensional temperature behind the shock wave, $\gamma RT_2/U_S^2$ (R is the gas constant per unit mass), versus B_1/B_0 for various values of θ and P.

In Figure 4, the negative tangent of the angle of downstream flow, in the laboratory reference frame, is shown, i.e. the ratio $-v_2/u_2$ in laboratory coordinates. (By the choice of sign convention this is a positive quantity.) In the transverse

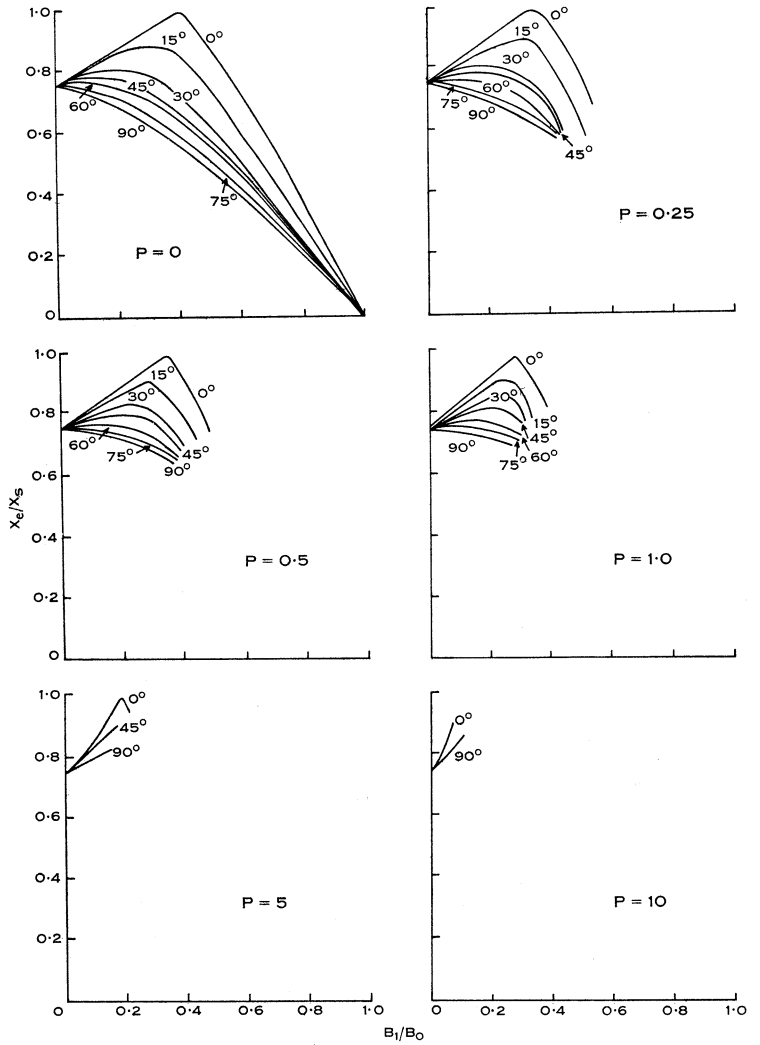

Fig. 7.—Ratio of distance travelled by the leading edge of the expansion wave, X_e, to distance travelled by the shock wave, X_S at a given time versus B_1/B_0 for various values of θ and P.

case there is no azimuthal flow at all, but as θ decreases the amount of rotation, or azimuthal flow, increases. For the normal shock in the switch-on region, the flow is increasingly rotational for increasing P, whereas under ordinary shock flow conditions the flow is entirely axial. Thus for the switch-on shock, a higher ionization will

be obtained by a flow in which there is as much rotation as possible. This explains the present interest in the study of rotating plasmas in thermonuclear research.

The density ratio ρ_2/ρ_1 across the shock front is a measure of the shock strength; this ratio is presented in Figure 5. In the ordinary gas dynamic limit ($B_1/B_0 = 0$) the density ratio is 4 for $P = 0$, and increases with increasing P. The curves are similar to those for B_2/B_1 in that stronger drive fields do not necessarily produce stronger shocks for a given P. We see that for $P \gtrsim 5$ an increase in drive field, with fixed initial field B_1, produces a decrease in shock strength.

As shown in Figure 6, greater downstream gas temperatures are produced by greater drive fields, at a fixed ionization level; also for a fixed T_2, greater drive fields produce higher ionization. The normal shock is capable of producing greater temperatures for a fixed drive field and ionization than the transverse shock, showing once again why the normal shock is perhaps of more interest than the transverse shock in plasma preparation. The $B_1/B_0 = 0$ limit of this quantity for $P = 0$ is 0·3125, and decreases slightly for increasing P.

Figure 7 graphs the ratio of the distance travelled by the leading edge of the expansion wave to the distance travelled by the shock front at a given time (X_e/X_S). When this ratio is greater than unity, the expansion wave leads the shock, producing an inherently unstable condition. However, this is not present here, although for $P = 0$ the expansion wave does catch the shock front for the normal shock at the transition point between the two flow regimes. In the neglected non-physical cases, X_e/X_S becomes complex. As for the ρ_2/ρ_1 curves, the X_e/X_S curves have maxima (regarded as a function of B_1/B_0) up to a certain P value, above which X_e/X_S becomes a strictly increasing function. The limit for $B_1/B_0 = 0$ increases slightly from its $P = 0$ value (0·75) for increasing P. Greater drive fields produce greater ionization when X_e/X_S is diminished.

Of interest to research workers in plasma preparation is the quantity $1-(X_e/X_S)$, which gives a measure of the length of the test gas region, i.e. the volume of the plasma produced.

In Figure 8 the profiles of various flow properties from the shock front (S) to the back wall are shown; they are shown for normal shock flow, two cases for each P value. The flow regions are designated: T = test gas region (region 2), E = expansion wave region, D = drive field region (region 0). The left-hand figure for each P value has the lower value of the parameter U_S/b_1 and is in the switch-on region of flow, whereas the right-hand figure for each P value lies in the ordinary shock region. As the pressure and density drop very rapidly away from their values in region 2, the test gas is well defined. The approximate linearity of the velocity components in the expansion wave, as noted in K.P., is evident here.

Figs. 8(a) to 8(l).—Profiles of flow properties between the shock front and the rear wall of the shock tube for $\theta = 0°$ and two values of the parameter U_S/b_1, so that the switch-on and ordinary flow regions are shown; S = shock front, T = test gas region (region 2), E = expansion wave region, D = drive field region (region 0). The profile numbers refer to flow properties as follows:
1 to $p/\rho_1 U_S^2$; 2 to U/U_S; 3 to $B^2/2\mu\rho_1 U_S^2$; 4 to $-v/U_S$; 5 to $(\rho/4\rho_1)^2$; 6 to $-E_Z/U_S B_{Y0}$.

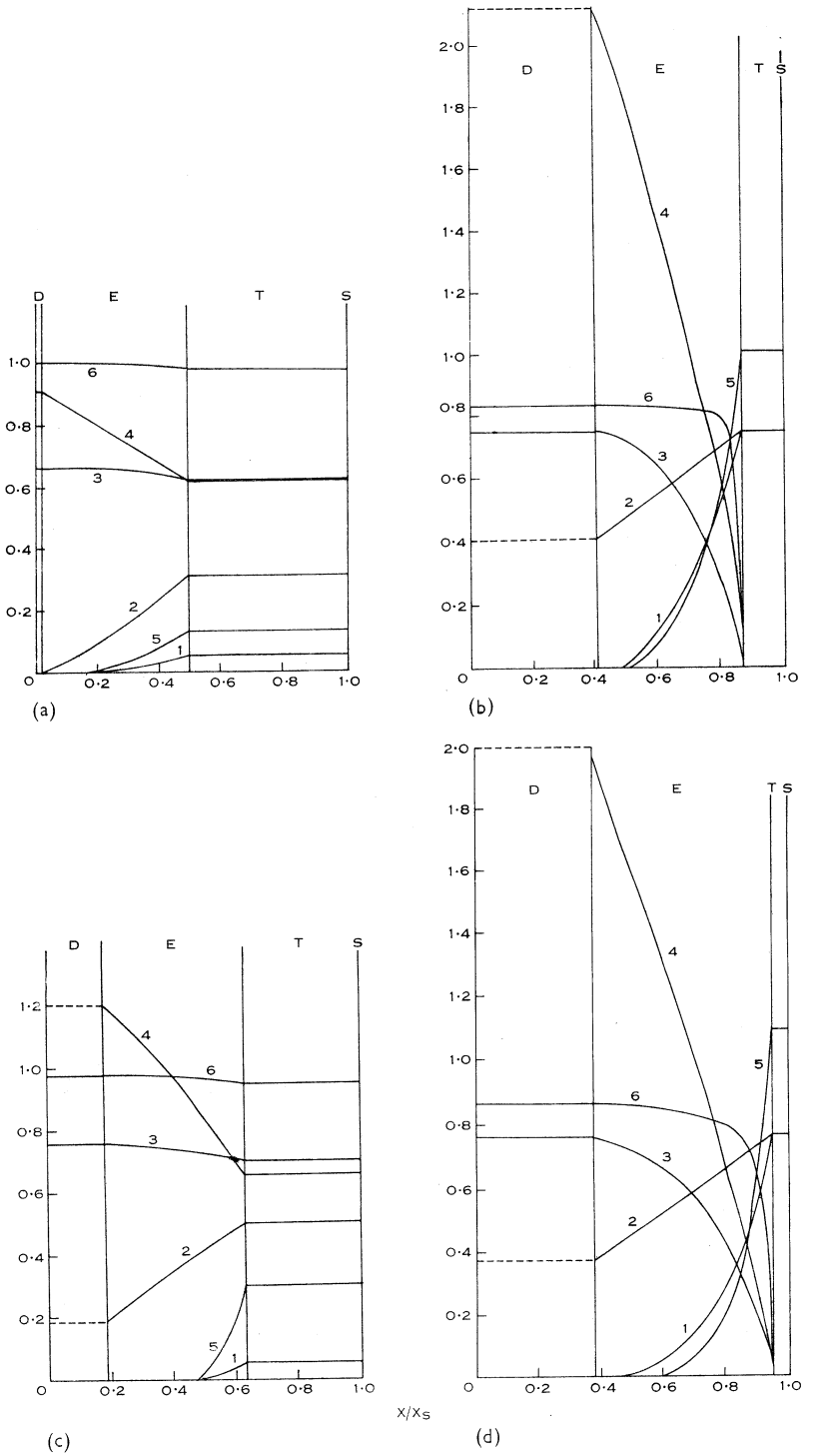

Fig. 8

(*a*) $P = 0$, $U_S/b_1 = 1{\cdot}2$; (*b*) $P = 0$, $U_S/b_1 = 4{\cdot}0$;
(*c*) $P = 0{\cdot}25$, $U_S/b_1 = 1{\cdot}5$; (*d*) $P = 0{\cdot}25$, $U_S/b_1 = 3{\cdot}5$.

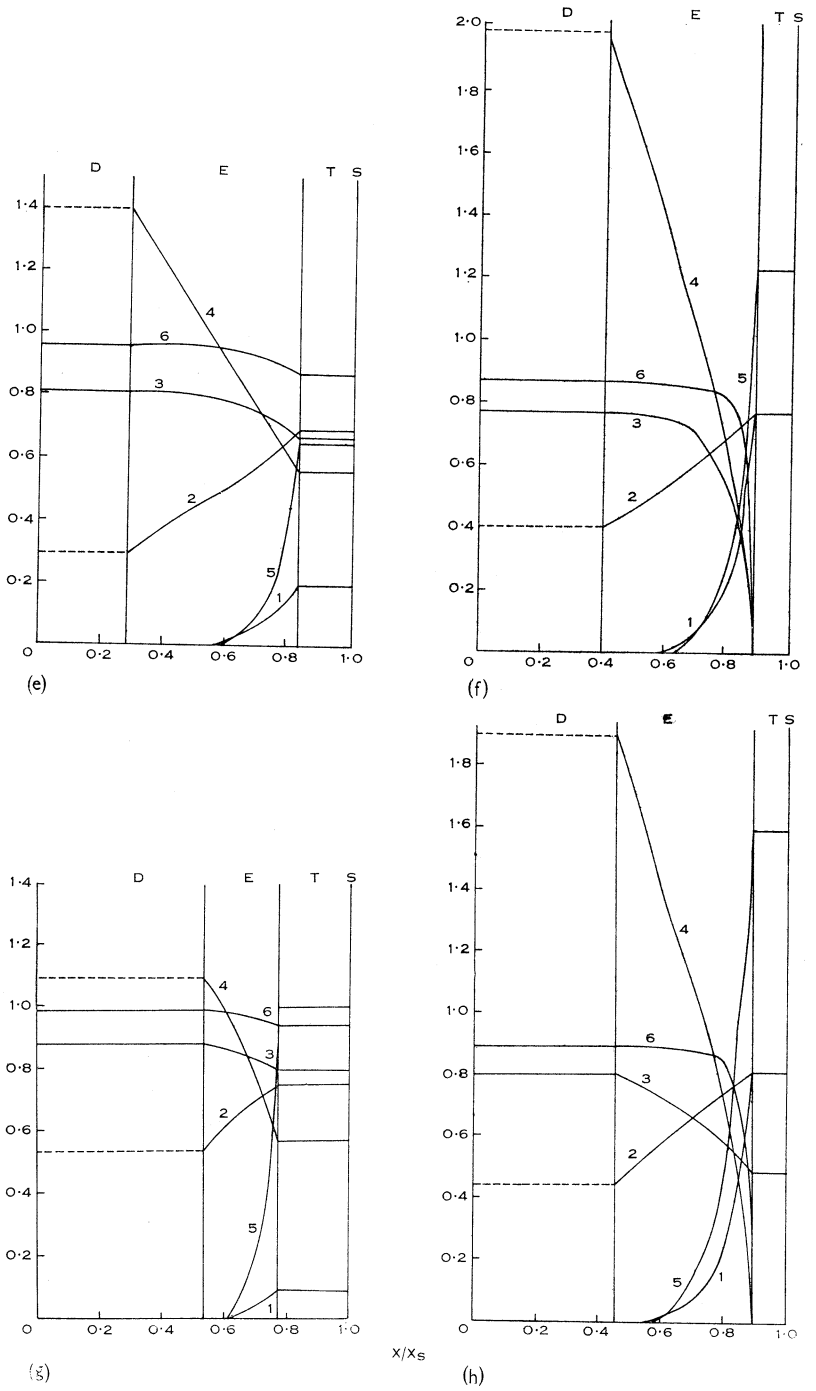

Fig. 8 (*Continued*)

(*e*) $P = 0{\cdot}5$, $U_S/b_1 = 1{\cdot}8$; (*f*) $P = 0{\cdot}5$, $U_S/b_1 = 3{\cdot}5$;
(*g*) $P = 1{\cdot}0$, $U_S/b_1 = 2{\cdot}0$; (*h*) $P = 1{\cdot}0$, $U_S/b_1 = 3{\cdot}5$.

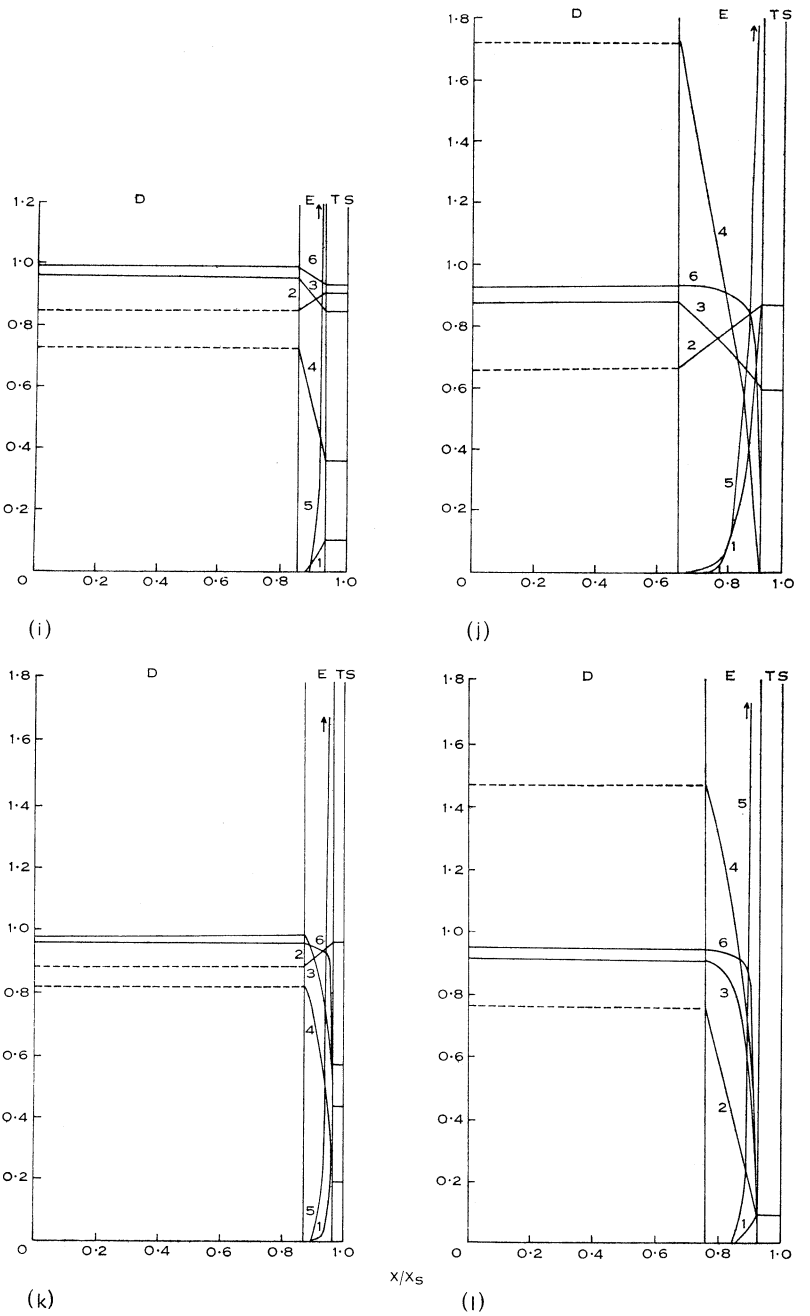

Fig. 8 (*Continued*)

(*i*) $P = 5$, $U_S/b_1 = 3{\cdot}5$; (*j*) $P = 5$, $U_S/b_1 = 5{\cdot}0$;
(*k*) $P = 10$, $U_S/b_1 = 4{\cdot}86$; (*l*) $P = 10$, $U_S/b_1 = 6{\cdot}0$.

Figure 9 essentially gives the radial (Z) component of the electric field at the electrode at the back of the tube as a function of B_1/B_0. This electric field can be used to calculate the impedance as seen by the circuit that drives the flow. For a

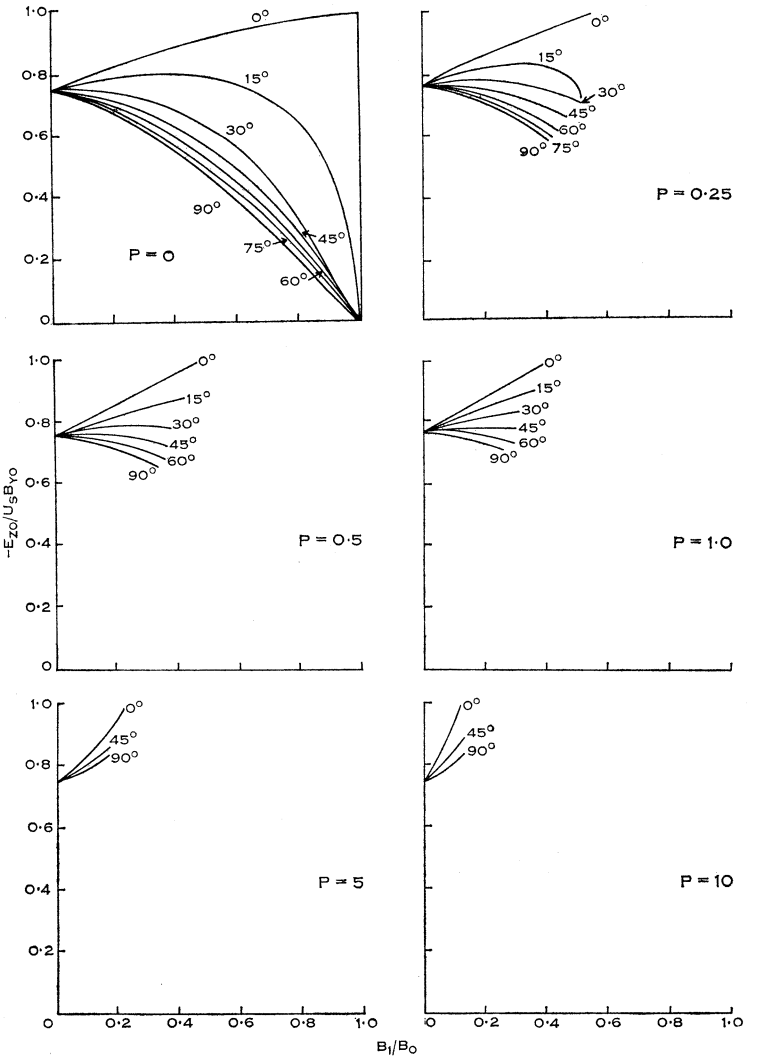

Fig. 9.—Non-dimensional electric field $-E_{Z0}/U_S B_{Y0}$, in the drive field region (region 0), versus B_1/B_0 for various values of θ and P.

fixed electric field, a greater magnetic drive field is required to produce greater ionization. The $B_1/B_0 = 0$ limit behaves with P in the same way as does that of Figures 7 and 10.

The axial component of the drive field gas velocity U_0 is considered as a function of B_1/B_0 in Figure 10. When it is not zero, the pressure and the density in this region must vanish to satisfy the zero axial mass motion boundary condition

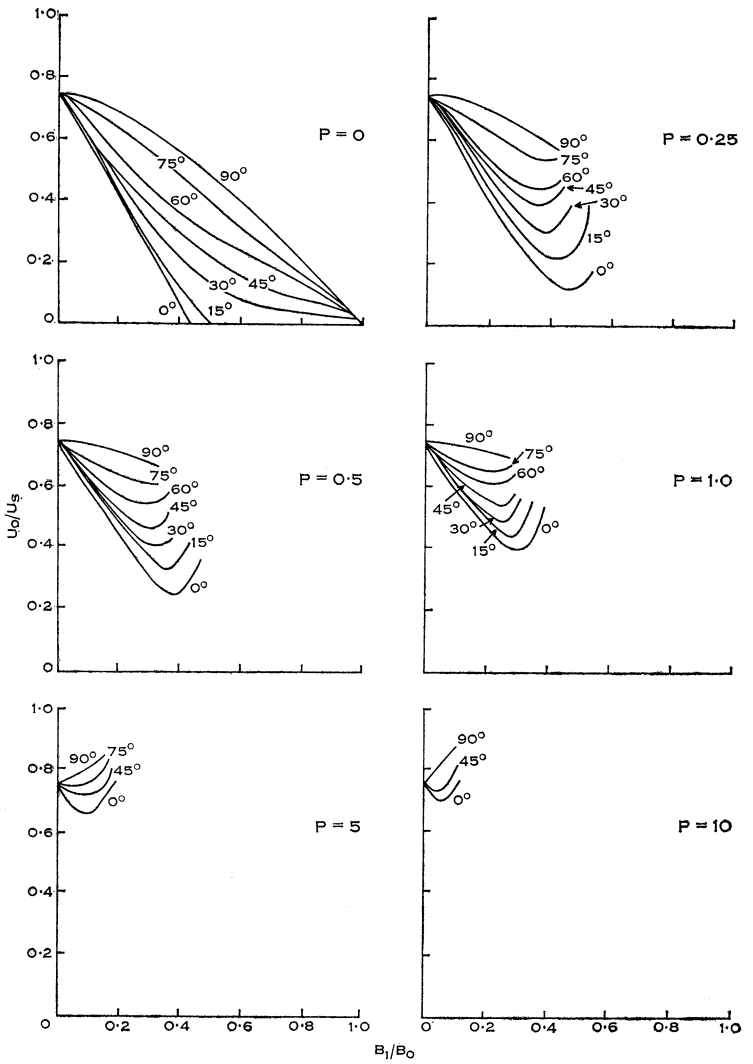

Fig. 10.—Non-dimensional axial component of gas velocity at the rear edge of the expansion wave, U_0/U_S, versus B_1/B_0 for various values of θ and P.

of the rear wall. When $U_0 = 0$, the pressure and density need not vanish, and the gas present remains in the region with no axial motion. As is shown in Figure 10, the condition $U_0 = 0$ is achieved only for $P = 0$; in all other cases there is a vacuum in the drive field region.

IV. Acknowledgments

The authors wish to thank Professor C. N. Watson-Munro for helpful discussion, and Professor H. Messel for the facilities provided. This work was supported in part by the Nuclear Research Foundation within the University of Sydney. One of us (B.G.) is the holder of a CSIRO Senior Post-graduate Studentship.

V. References

Bazer, J. (1958).—*Astrophys. J.* **128**: 686.

Chu, C. K. (1964).—*Physics Fluids* **7**: 1349.

Gross, R. A., and Kunkel, W. B. (1962).—"Plasma Hydromagnetics." (Ed. D. Bershader.) p. 58. (Stanford Univ. Press.)

Kemp, N. H., and Petschek, H. E. (1959).—*Physics Fluids* **2**: 599.

Kulikovski, A. G., and Lyubimov, G. A. (1960).—*Sov. Phys. Doklady* **4**: 1185.

Lehnert, B. (1958).—I.A.U. No. 6, p. 50.

May, R. M., and Tendys, J. (1965).—*Nucl. Fusion* **5** (2): (In press.)

Taussig, R. (1964).—Plasma Laboratory Reports, Nos. 12, 14, Columbia University.